Modal Test/Analysis Correlation for the Centaur G Prime Launch Vehicle

J. Chen,* T. Rose,* M. Trubert, B. Wada†
Jet Propulsion Laboratory, California Institute of Technology, Pasadena, California
and
F. Shaker*
NASA Lewis Research Center, Cleveland, Ohio

A modal test was performed on the Centaur G Prime launch vehicle for the purpose of verifying the loads analysis model. This paper describes the procedure by which the modal parameters obtained in this test were correlated with the corresponding analytical predictions. Based on this correlation, the stiffness model of the Shuttle trunnion system has been modified. The evolution of the model updating and the final results are described.

Introduction

FOR aerospace payload structural systems in which the responses and loads dictate the design and thus the size and weight of the structure, the accuracy of the analytical model is of major importance because of the stringent weight constraints. A test-verified analytical model is usually required for the final verification loads analysis. The modal test from which the natural frequencies, mode shapes, modal damping, and other dynamic characteristics are determined experimentally is used to verify the analytical model. The comparison of various modal characteristics, such as the natural frequencies and mode shapes obtained from the modal test and its corresponding analytical predictions, define the accuracy of the analytical model. The modal test should be designed in such a way that these dynamic characteristics can be readily measured from the test. In addition to predicting the eigenvalues and eigenvectors, the analysis can yield other valuable information that can be used as criteria for the verification of the model.

The Centaur G Prime launch vehicle was the upper stage for the upcoming Galileo and Ulysses interplanetary spacecraft and would have been launched by the Space Shuttle prior to the Challenger accident. The modal test of the Centaur G Prime cargo element was conducted in July–August 1985. Figure 1 shows the schematics of the Centaur G Prime in its modal test configuration. Although several different methods were used in the modal test, the results of the high-level sine dwell method were chosen for the correlation and model updating.

Pretest Analysis and Test/ Analysis Model (TAM)

In general, the number of degrees of freedom in the loads analysis model is orders of magnitude greater than the number of measurements to be made during testing. For test/analysis correlation, one may use these limited measurements to extrapolate and map the motions of the entire loads analysis model consisting of all the degrees of freedom. On the other hand, a condensed model can be constructed such that its degrees of freedom will be compatible with the test measurements. This condensed model is called the test/analysis model (TAM), whose purpose is to relate the test-measured results to the analytical predictions and to assist in the test data reduction.

Much smaller than the loads analysis model, the TAM can provide a cost-effective way of performing the pretest analysis. The TAM must be constructed so that all of the modal characteristics predicted by the loads analysis model can be reproduced by the TAM within the range of interest. Specifically, the choice of the TAM degrees of freedom must have sufficient resolution to represent the "important" (mode) shapes and the TAM-predicted frequencies and effective mass must be in agreement with those of the loads analysis model. Figure 2 shows the finite-element loads analysis model of a test article having approximately 30,000 degrees of freedom. After considerable evolution, the TAM model was established with the degrees of freedom corresponding to the mode shape measurements, i.e., 127 accelerometer measurements.

Table 1 shows the modal analysis results from the full-size loads model. The primary modes were identified based on the effective mass distribution. These primary modes are important to the loads analysis and will be verified by the modal test. Table 2 shows the evolution of the TAM prior to the test and

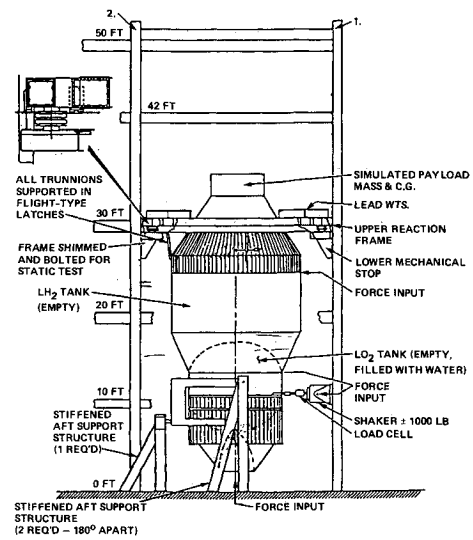

Fig. 1 Centaur G Prime in modal test configuration.

Received March 17, 1986; presented as Paper 86-1002 at the AIAA/ASME/ASCE/AHS 27th Structures, Structural Dynamics and Materials Conference, San Antonio, TX, May 19–21, 1986; revision received Oct. 10, 1986. Copyright © American Institute of Aeronautics and Astronautics, Inc., 1987. All rights reserved.

*Member AIAA.
†Deputy Manager, Applied Technology Section. Member AIAA.
‡Senior Structural Dynamics Engineer, Space Transportation Engineering Division.

Table 1 Centaur G prime mode description

Mode	Frequency, Hz	Effective mass X	Y	Z	Description
1[a]	4.76	0	41,154	0	1st yaw
2[a]	5.85	37,219	0	9,078	1st axial and pitch
3[a]	7.15	11,707	0	29,443	2nd pitch and axial
4[a]	7.81	0	2,126	0	GLL yaw
5[a]	10.97	46	0	6,499	GLL pitch
6	13.35	0	0	54	CSS yoke mode
7	15.57	0	0	0	Upper reaction frame
8	15.92	0	199	0	Engine in yaw
9	16.40	2	91	0	Engine in yaw
10[a]	16.87	1	2,412	0	CSS yaw
11	20.91	20	10	68	Engine pitch
12	21.41	0	16	22	Engine pitch and yaw
13	23.18	5	442	0	Centaur bending

[a]Identified as primary modes.

Table 2 TAM frequency comparison, Hz

Mode	GDC (32,000)	TAM 1.1 (648)	TAM 4.0 (144)	TAM 7.0 (81)	TAM 14.0 (127)
1[a]	4.76	4.85	4.85	4.85	4.84
2[a]	5.85	5.88	5.88	5.88	5.98
3[a]	7.15	7.30	7.30	7.30	7.40
4[a]	7.81	7.84	7.84	7.84	7.52
5[a]	10.97	10.96	10.97	10.98	10.39
6	13.35	13.49	13.51	13.52	13.76
7	15.57	15.58	15.58	15.59	—
8	15.92	—	—	—	—
9	16.40	—	—	—	—
10[a]	16.87	16.80	16.85	16.89	17.20
11	20.91	19.86	19.91	19.92	—
12	21.41	—	—	—	—
13	23.18	23.79	23.91	24.08	24.50

[a]Identified as primary modes.

its comparisons with the loads model. The TAM results indicate an accurate modal representation of the loads model, especially for the primary modes.

Correlation Parameters

It is important that the accuracy requirement for the analytical model be defined prior to the test/analysis correlation. Very little has been done to establish the degree of correlation required between the mathematical model and the test data. Initial efforts[1,2] produced some obvious insights that are often not considered during a test. Also, investigations related to the modal parameter correlation can be found in previous studies.[3,4] Usually, measurements from a modal test include natural frequencies, mode shapes, modal damping, and modal forces in structural members. These quantities are obtained directly if the traditional multishaker sine dwell method is used in the modal test. Otherwise, these values are estimated from curve fitting the frequency response functions for the modern modal test methods. In analysis and test correlation for the purpose of validating the finite-element model, additional parameters should be considered in the comparison.

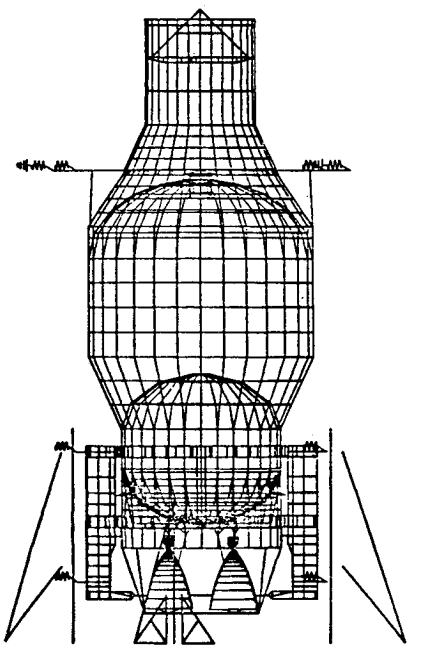

Fig. 2 Centaur G Prime finite-element modal.

Table 3 Cross-orthogonality

Analytical mode	Test Mode 1	2	3	4	5	6	7
1	−9.74E−1	−2.33E−2	−2.83E−1	5.60E−3	−7.23E−3	2.95E−2	8.20E−2
2	−1.67E−1	8.68E−3	9.34E−1	−1.00E−2	5.28E−2	−5.27E−3	8.46E−2
3	−2.99E−2	−8.80E−1	3.38E−2	−1.06E−1	2.49E−1	5.23E−3	−3.31E−2
4	1.78E−2	1.49E−1	4.58E−4	−9.70E−1	1.11E−1	−3.57E−2	1.53E−1
5	−2.04E−2	7.39E−2	6.39E−3	1.73E−1	9.56E−1	1.89E−2	2.08E−2
6	−8.62E−4	1.07E−2	3.16E−3	−1.78E−2	−1.93E−2	−6.56E−3	−2.82E−1
7	4.16E−3	−4.83E−3	−7.11E−3	4.39E−3	−2.49E−3	5.56E−2	−2.68E−1
8	1.90E−2	8.49E−4	−4.48E−2	−3.36E−4	−7.23E−3	9.15E−1	−8.09E−2
9	1.86E−2	1.54E−3	−1.36E−1	−3.78E−3	−3.61E−3	−3.27E−1	3.06E−1
10	−8.86E−3	−4.44E−3	4.85E−2	−3.01E−3	8.61E−3	−1.36E−2	6.36E−2
11	−1.59E−2	2.19E−3	1.80E−2	−2.97E−3	9.31E−4	−4.72E−2	2.97E−3
12	7.03E−3	−1.56E−2	1.14E−2	−2.24E−2	4.45E−3	2.23E−2	7.72E−1
13	−4.87E−2	1.25E−3	4.04E−2	−3.89E−3	3.09E−3	1.15E−1	1.17E−1
14	−1.33E−2	4.91E−3	−5.08E−3	−6.38E−3	4.08E−4	2.63E−2	2.13E−2
Column Maxima	9.74E−1	8.80E−1	9.34E−1	9.70E−1	9.56E−1	9.15E−1	7.72E−1
Correlated Analytical Modes	1	3	2	4	5	8	12

Table 4 Frequency comparison

Mode	Test Hz	Mode	Analysis Hz	Error,%	Mode description
1	4.4098	1	4.1112	−6.77	Roll at keel pins 410Y, 800 lb full
2	7.8696	3	7.1572	−9.05	Forward pitch 500 lb 409Z, repeat
3	7.6596	2	7.0037	−8.56	Forward yaw 800 lb driver, 411Y full
4	8.2196	4	7.5847	−7.72	Axial mode 1000 lb 404X-
5	9.1895	5	8.4548	−8.00	Aft center pitch 750 B 408Z-
6	20.2490	8	21.3893	5.63	Engine lateral, door part 410Y, 800 lb full
7	27.8785	12	27.0513	−2.97	Aft bulkhead bulge, 404X, 800 lb

Table 5 Orthogonality of test modes

Mode	1	2	3	4	5	6	7
1	1.000	0.009	0.104	0.020	−0.030	−0.031	−0.076
2		1.000	−0.025	−0.042	−0.125	−0.011	−0.044
3			1.000	−0.018	0.067	0.013	0.021
4				1.000	0.036	0.033	−0.149
5					1.000	0.011	0.043
6						1.000	−0.164
7							1.000

Table 6 Test effective mass

Mode	Frequency, Hz	Effective mass X	Y	Z	θX	θY	θZ
1	4.4098	9.293E+00	4.188E+04	1.390E+01	7.012E+09	3.981E+07	5.155E+10
2	7.8696	2.223E−02	1.430E+01	3.964E+04	4.959E+06	4.456E+10	1.515E+07
3	7.6596	1.066E+00	2.207E+03	4.741E+01	3.168E+08	4.932E+07	6.080E+09
4	8.2196	4.980E+04	1.459E+01	4.502E+02	1.875E+06	1.350E+10	2.233E+07
5	9.1895	7.442E+02	1.753E+01	1.414E+04	2.787E+06	2.073E+10	3.518E+07
6	20.2490	5.381E+01	1.028E+03	8.996E−01	1.377E+08	1.720E+07	1.501E+09
7	27.8785	9.998E+02	1.699E+00	4.761E+01	1.937E+07	4.022E+08	1.993E+06
Total		5.161E+04	4.516E+04	5.433E+04	7.495E+09	7.930E+10	5.921E+10

Table 7 Analytical effective mass

Mode	Frequency, Hz	Effective mass X	Y	Z	θX	θZ	θT
1	4.1112	2.242E−03	3.512E+04	2.974E−02	5.784E+09	2.003E+04	4.104E+10
2	7.0037	8.918E−01	6.972E+03	1.426E−03	1.170E+09	2.307E+05	1.339E+10
3	7.1572	1.381E+03	6.820E−02	3.643E+04	8.539E+03	3.734E+10	7.926E+04
4	7.5847	4.790E+04	2.044E−02	8.432E+02	3.339E+03	1.398E+10	4.873E+04
5	8.4548	4.009E+01	2.263E−01	5.653E+03	2.317E+04	1.205E+10	3.911E+05
6	13.9512	1.465E+02	2.122E−02	2.850E+02	1.806E+03	5.305E+08	3.699E+04
7	20.3078	1.415E−01	1.801E−01	4.063E+01	2.550E+03	6.819E+07	2.083E+05
8	21.3893	1.354E−01	3.283E+01	1.206E−02	2.029E+06	8.399E+04	4.180E+07
9	22.1193	1.467E−01	1.739E+03	5.152E−02	1.212E+08	2.209E+05	2.541E+09
10	24.9359	1.190E+01	2.577E+02	3.033E−01	3.189E+07	4.567E+05	4.019E+08
11	25.9034	5.306E−03	1.192E+02	1.020E−01	2.643E+07	1.378E+05	2.296E+08
12	27.0513	2.632E+01	5.431E+00	1.117E−01	1.103E+06	5.404E+06	8.831E+06
13	28.8175	3.644E+00	1.707E+02	8.684E−01	6.857E+07	1.781E+05	3.411E+08
14	30.7120	4.469E−02	4.771E+00	3.359E−03	1.449E+06	4.224E+04	6.865E+06
15	32.3133	6.907E−02	6.939E−03	8.219E−01	2.974E+03	1.692E+06	5.116E+03
16	34.1363	6.095E−02	1.658E+02	2.426E+00	1.875E+07	3.454E+06	3.044E+08
17	34.8832	4.535E−03	5.325E+00	5.134E+02	9.940E+05	8.675E+08	7.331E+06
18	35.7645	4.149E+03	1.416E+03	3.104E−03	2.071E+08	1.616E+05	2.055E+09
Total		4.951E+04	4.601E+04	4.377E+04	7.433E+09	6.485E+10	6.037E+10

These additional parameters can be obtained by using the TAM and postprocessing the test data. The procedure of performing test/analysis correlation will now be described and the reasons for selecting certain parameters for the comparison will be given. However, the mathematical derivation of the parameters can be found in Ref. 5.

Mode Identification (Cross Orthogonality)

Prior to any correlation, the identification of the test mode with the corresponding analytical mode is required. This can be achieved by examining the cross orthogonality between the test and analytical modes. Table 3 shows the cross orthogonality between the modes from the TAM 41F and the modes obtained from the high-level sine dwell test for the same configuration. The identification is made by establishing the largest term between a test mode and all of the analytical modes. The smallness of the value from the other uncorrelated modes is an indication of the linear independence of the test mode and uncorrelated analytical modes.

Frequency

The test-measured data and the analytically predicted values of frequency can be compared directly. Frequency correlation is considered very essential; at a minimum, a valid model must be able to predict accurate natural frequencies. Table 4 shows a typical frequency comparison obtained from the Centaur G Prime modal test.

Orthogonality

Any errors in the mode shape measurements and/or TAM mass representation will produce finite off-diagonal terms in the orthogonality check. It is common practice that a good correlation between test and analysis should produce off-

Table 8 Mode shape comparisons of GLL in yaw

Description	DOF	Analysis 2 7.004 Hz	Test 3 7.660 Hz
GLL in *Y*	26	1.000*E*+00	1.000*E*+00
GLL/JPL, adapter, *Y*	101	6.514*E*−01	7.888*E*−01
GLL/centaur adapter, *Y*	48	4.546*E*−01	6.381*E*−01
Right forward trunnion, *Y*	2	4.658*E*−01	5.836*E*−01
GLL Centaur adapter *Y*	55	4.633*E*−01	5.562*E*−01
Left forward trunnion, *Y*	5	4.660*E*−01	5.531*E*−01
Engine supp., *Y*	32	−6.276*E*−01	−4.498*E*−01
Stub adapter, *Y*	58	1.535*E*−01	4.418*E*−01
Right engine bell, *Y*	97	−6.522*E*−01	−4.327*E*−01
Engine supp., *Y*	34	−6277*E*−01	−4.225*E*−01
Right engine c.e., *Y*	43	−6.457*E*−01	−4.222*E*−01
Left engine bell, *Y*	98	−7.422*E*−01	−4.147*E*−01
Left engine bell, *Y*	45	−6.449*E*−01	−4.027*E*−01
Right engine gimbal, *Y*	122	−5.962*E*−01	−3.992*E*−01
Left engine gimbal, *Y*	119	−5.963*E*−01	−3.946*E*−01
Stub adapter	61	3.614*E*−01	3.811*E*−01
Aft dep. adapter, *Y*	88	−8.150*E*−01	−3.775*E*−01
Left forward trunnion, *X*	4	−3.794*E*−01	−3.507*E*−01
Stub adapter *X*	59	−3.661*E*−01	−3.443*E*−01
GLL/Centaur adapter *X*	54	3.295*E*−01	3.325*E*−01
RSS error		1.177*E*−02	

Table 9 Shape comparisons of axial mode

Description	DOF	Analysis 4 7.585 Hz	Test 4 8.220 Hz
GLL/Centaur int., *X*	47	8.062*E*−01	1.000*E*+00
Forward LHZ ring, *X*	63	7.918*E*−01	9.499*E*−01
GLL/JPL, adapter	100	8.504*E*−01	9.473*E*−01
Stub adapter, *X*	61	8.720*E*−01	9.466*E*−01
Left engine gimbal, *X*	118	9.989*E*−01	9.437*E*−01
GLL/JPL adaptor, *X*	24	8.996*E*−01	9.358*E*−01
Right engine gimbal, *X*	121	1.000*E*+00	9.261*E*−01
Forward transmission ring, *X*	69	7.856*E*−01	9.258*E*−01
GLL/Centaur, int., *X*	54	8.818*E*−01	9.234*E*−01
GLL/Centaur, int., *X*	57	7.946*E*−01	9.179*E*−01
GLL/JPL adapter, *X*	22	8.962*E*−01	9.162*E*−01
Forward LOZ ring, *X*	75	8.003*E*−01	9.155*E*−01
Aft LOZ ring, *X*	81	8.145*E*−01	8.976*E*−01
Right forward adapter, *X*	1	8.532*E*−01	8.975*E*−01
GLL/Centaur int., *X*	50	8.769*E*−01	8.941*E*−01
Aft dep. adapter	87	8.217*E*−01	8.849*E*−01
Forwad LHZ ring, *X*	65	8.493*E*−01	8.810*E*−01
Forward transmission ring, *X*	71	8.380*E*−01	8.726*E*−01
Forward LHZ ring, *X*	67	8.674*E*−01	8.674*E*−01
Stub adapter, *X*	59	8.542*E*−01	8.633*E*−01
RSS error		8.386*E*−02	

Table 10 Kinetic energy distribution

Test mode 3, forward yaw 800 lb drive. 411Y full, 7.6596 Hz frequency

SE		Degrees of freedom X	Y	Z	Sum
1	GLL Spacecraft		7.2394E−01	2.5508E−04	7.2420E−01
2	JPL adapter	4.5765E−04	6.0536E−02	1.2341E−03	6.2228E−02
4	Central forward adapter	2.8375E−03	2.8771E−02	7.3852E−04	3.2347E−02
6	Liquid hydrogen tank	5.0866E−03	2.6424E−03	1.8072E−05	7.9097E−03
8	Engine 1	7.1949E−04	4.8190E−02	4.8194E−05	4.8958E−02
9	Engine 2	1.6384E−03	4.5920E−02	2.3539E−04	4.7794E−02
10	Lo_x tank	2.5612E−03	2.1111E−02	3.5781E−04	2.4030E−02
11	Launch adapter	2.8977E−04	1.1216E−02	3.7097E−05	1.1543E−02
12	CSS structure	3.4496E−04	9.3784E−03	6.4841E−06	9.7298E−03
14	Test fixture	7.0769E−04	1.9220E−02	8.3000E−04	2.0758E−02
	Sum	1.4643E−02	9.7093E−01	3.9234E−03	

Analytical Mode 2. 7.0037 Hz frequency

SE		Degrees of freedom X	Y	Z	Sum
1	GLL Spacecraft		4.7644E−01	1.6926E−06	4.7644E−01
2	JPL adapter	2.5270E−4	2.7106E−02	3.2524E−04	2.7684E−02
4	Central forward adopter	1.9822E−03	1.0419E−02	4.5980E−04	1.2861E−02
6	Liquid hydrogen tank	4.2747E−03	2.1010E−03	1.7550E−03	8.1307E−03
8	Engine 1	1.1685E−03	7.1567E−02	3.5857E−04	7.3095E−02
9	Engine 2	1.3173E−03	7.0970E−02	3.6208E−04	7.2649E−02
10	Lo_x tank	2.0093E−03	9.7609E−02	7.5758E−03	1.0719E−01
11	Launch adapter	4.7649E−04	3.2834E−02	4.4667E−04	3.3757E−02
12	CSS structure	2.3021E−04	5.8756E−04	1.2257E−04	9.4034E−04
14	Test fixture	9.4267E−07	1.1290E−04	2.2035E−06	1.1605E−04
	Sum	1.1712E−02	7.8974E−01	1.1410E−02	

Table 11 Kinetic energy distribution

Test mode 4, axial mode 1000 lb 40 ax-frequency 8.2196 Hz

SE		Degrees of freedom X	Y	Z	Sum
1	GLL spacecraft		1.5890E−04	4.7308E−03	4.8897E−02
2	JPL adapter	5.1723E−02	1.8511E−05	1.1304E−03	5.2872E−02
4	Central forward adapter	1.8613E−02	1.6410E−05	7.1250E−05	1.8701E−02
6	Liquid hydrogen tank	1.3109E−02	4.3486E−06	5.9149E−05	1.3173E−02
8	Engine 1	9.4705E−02	7.4031E−05	1.7056E−03	9.6484E−02
9	Engine 2	9.7447E−02	5.8972E−05	8.3149E−04	9.8338E−02
10	Lo_x tank	2.6185E−02	1.1981E−04	4.1994E−03	3.0504E−02
11	Launch adapter	1.0275E−02	6.0863E−05	9.3170E−04	1.1268E−02
12	CSS structure	6.6437E−03	8.9657E−04	1.2355E−04	7.6638E−03
14	Test fixture	1.9586E−03	1.2765E−02	7.2966E−04	1.5453E−02
	Sum	3.2066E−01	1.1573E−02	1.4513E−02	

Analytical Mode 4. 7.5847 Hz frequency

SE		Degrees of freedom X	Y	Z	Sum
1	GLL spacecraft		7.1331E−06	2.1563E−02	2.1571E−02
2	JPL adapter	4.2645E−02	2.6858E−07	3.5240E−03	4.6169E−02
4	Central forward adapter	1.6802E−02	3.0163E−06	1.3595E−03	1.8165E−02
6	Liquid hydrogen tank	1.1158E−02	1.1500E−07	6.8852E−04	1.1847E−02
8	Engine 1	1.0566E−01	1.9276E−06	1.8281E−04	1.0585E−01
9	Engine 2	1.0448E−01	1.1301E−05	8.5034E−05	1.0457E−01
10	Lo_x tank	2.2700E−02	3.2420E−06	4.1380E−03	2.6841E−02
11	Launch adapter	9.6580E−03	3.2444E−05	2.2251E−04	9.9129E−03
12	CSS structure	3.6520E−03	7.0128E−04	4.8038E−05	4.4013E−03
14	Test fixture	2.5600E−06	1.4343E−05	4.9987E−06	2.1901E−05
	Sum	3.1676E−01	7.7507E−04	3.1817E−02	

diagonal terms which are less than 10% of those diagonal terms. Table 5 shows a typical orthogonality check for some of the experimental modes measured in the Centaur G Prime modal test.

Effective Mass

The comparison of effective mass with the rigid-body mass can be used as an indication of the completeness of the modes extracted, as well as the importance of each individual mode in the loads analysis. Tables 6 and 7 show such a comparison from the Centaur G Prime modal test.

Mode Shape

The agreement or disagreement of the mode shape comparison is a direct indication of the accuracy of the analytical model. Table 8 compares analytical mode shape 2 with test mode shape 3. The comparison indicates excellent agreement, not only in the general shape such as the overall yaw motion of the mode, i.e., Y direction, but also the modal amplitude for the degrees of freedom with large motion. The root-sum-square (rss) error of the comparison over 127 measurements is 0.01177, which is two orders of magnitude smaller than the maximum amplitude. Table 9 shows mode shape comparison for the axial modes. Although agreement similar to that of Table 8 is obtained, the accuracy of the analytically predicted

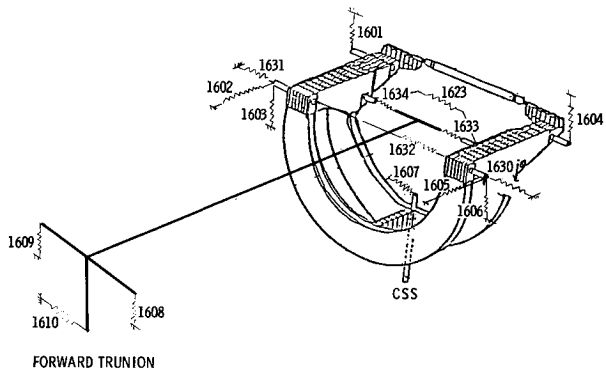

Fig. 3 Shuttle trunnion stiffness system.

Table 12 Frequency summary for various trunnion lock conditions[a]

Mode	Frequency, Hz			
	BC 1	BC 2	BC 3	BC 4
1	4.87	4.74	4.89	5.42
2	7.15	5.85	7.27	7.33
3	7.16	7.15	8.27	8.54
4	8.20	7.81	8.37	12.19
5	10.95	10.94	10.97	13.45
6	13.51	13.35	15.58	15.58
7	15.58	15.58	16.10	16.10
8	16.03	15.59	16.44	16.44
9	16.43	16.41	20.97	20.97
10	20.83	16.87	21.44	21.45

[a]BC 1: Trunnions carrying dead weight DOF constrained. BC 2: All trunnion DOF sliding. BC 3: BC 1 + trunnion DOF carrying offset moments constrained. BC 4: All trunnion DOF constrained.

Table 13 TAM 41F configuration for lox tank (mass off-loaded 5000 lb in Y and Z)

CFLA52	Value	CFLA52	Value
Trunnion springs		CSS springs	
1601	$28.0E+6$	1623	$1.5E+8$
1602	$45.3E+6$	1632	$0.5E+6$
1603	$19.1E+6$		
1604	$28.0E+6$	Interface springs	
1605	$45.3E+6$	1633	$5.0E+4$
1606	$19.1E+1$	1634	$5.0E+4$
1607	$28.0E+6$		
1630	$2.0E+5$	Forward trunnion springs	
1631	$2.0E+5$	1608	$7.5E+4$
		1609	$7.5E+4$
		1610	$3.8E+4$

Table 14 Outline of TAM

Test	Description
1.1	Baseline TAM—starting point—all accelerometer grids plus selected grids (648 degree-of-freedom, DOF)
3	Major c.g. and accelerometer DOF (276 DOF)
3.1	TAM 3 with modified test support structure (285 DOF)
4	Baseline TAM with 2% or more kinetic-energy DOF retained (144 DOF)
5	Baseline TAM with forward trunnions released
6	Major c.g. DOF only (78 DOF)
6.1	TAM 6 with modified support structure
7	Similar to TAM 4 but for first 20 modes
7.1	TAM 7 with empty Lo_x tank
8	TAM 6 DOF plus adapter interface and trunnion DOF
9	TAM 4 with support structure fixed
10	TAM 9 + c.g. dof
11	Accelerometer DOF only and selected DOF
11C	Accelerometer DOF only (empty and full)
12	Accelerometer and major c.g. DOF only
13	TAM 12 with modified forward trunnion springs
14	TAM 11 with support structure constrained
14C	TAM11C with support structure constrained
15	TAM11C plus engine c.g. DOF for Lo_x full and empty configuration
15P4	TAM 15 with all trunnions constrained
16	TAM 15 with modified trunnion stiffness for Lo_x tank empty configuration
17	TAM 16 with modified trunnion stiffness for Lo_x empty configuration
18	TAM 17 with modified trunnion stiffness
19	TAM 18 with modified trunnion stiffness
20	TAM 19 with modified trunnion stiffness
21	TAM 20 with modified trunnion stiffness for full and empty Lo_x tank configuration
22	A spring added to Centaur support structure
23	TAM 21 with model correction from GDC
24	TAM 23 with modified trunnion stiffness
25	TAM 21 with selected trunnion constrained
26	TAM 21 with diagonal mass matrix
27	TAM 21 with modified trunnion stiffness in axial direction
28	TAM 27 with modified trunnion stiffness
29	TAM 28 with modified trunnion stiffness
30	TAM 29 with modifed trunnion stiffness
31	TAM 30 with modified trunnion stiffness in pitch directions
32	TAM 31 Lo_x tank full configuration but off-loaded in Y and Z by 5000 lb
33	TAM 31 with Lo_x tank off-loaded by 10,000 lb in Z only
34	TAM 32 with modified trunnion stiffness
35	TAM 34 with modified trunnion stiffness
36	TAM 32 with modified trunnion stiffness
37	TAM 36 with modified trunnion stiffness
38	Model error, discarded
39	Model error, discarded
40	TAM 37 with modified trunnion stiffness
41	TAM 40 with modified trunnion stiffness, final TAM
41B	TAM 41 with modified trunnion stiffness
43E	TAM 41 with empty Lo_x tank and trunnion constrained
43F	TAM 41 with trunnion constrained

mode shape is not as good as in the previous case, as indicated by a higher rss error.

Local Kinetic Energy

The local kinetic energy distribution can be used to identify the nature of the modes. The higher kinetic energy is associated with the degrees of freedom with either large mass or large modal displacement, or both. The comparison provides a good indication of which item in the model should be modified in order to achieve better correlation.

Table 10 shows the local kinetic energy distribution comparison for analytical mode 2 and test mode 3. Both modes show large energy in the yaw Y direction. However, a discrepancy is found in the Galileo spacecraft where results show 72% of the energy as compared to only 47% in the analytical model. The modeling error is most likely in the adapter that connects the Galileo spacecraft to the Centaur G Prime launch vehicle or in the forward test supports.

Table 11 shows the comparison of the kinetic energy distribution between the test mode 4 and analytical mode 4. Both indicate an axial mode with approximately 10% of energy concentrated at each engine. It is probable that the models for the engine support are quite representative.

Model Updating

One of the most important uncertainties in the model is the mathematical representation of the trunnions in the Shuttle cargo bay. Although the trunnions are designed as energy-dissipation devices, namely, frictional dampers, they also provide added stiffness. The frictional damping is provided by the sliding of the components across the trunnion. However, this sliding does not necessarily occur all the time. It slides at large-amplitude response and becomes locked at small-amplitude response, i.e., a nonlinear phenomenon. Table 12 shows the frequency differences for the various trunnions in either the sliding or locked configuration.

It was decided to model the effects of the trunnion friction by varying the stiffness at the trunnion support in such a way that the modal parameters were correctly simulated. To properly model these trunnion stiffnesses and their effects on damping became an important issue for the Space Shuttle payload loads analyses.[6-8] The effects of trunnion friction is important in the low-frequency modes, which are also the important modes for the loads analyses. Figure 3 is a schematic of the Centaur G Prime vehicle supported by the trunnion springs. Based on a comparison of the TAM results and modal test data, these springs are adjusted to optimize the modal parameter correlation. Table 13 shows the adjusted trunnion springs for the final model (TAM 41F), which is the 41st version for a configuration with the oxidizer tank full.

The previously shown comparisons and correlations between the analysis and test are based on the TAM 41F. Every version of the TAM was constructed for a particular purpose and the entire process of the TAM evolution took approximately 12 months. A brief description is provided for each TAM in Table 14.

Conclusions

It is well-known that the trunnion/latch assemblies are inherently nonlinear. During the test, it was observed that modal characteristics are indeed functions of the response level for several modes. Questions have been raised as to the conditions under which the test should be conducted and whether its results can be used to verify a linear loads model. Since the loads are transmitted through the interfaces, namely, the trunnion/latch assemblies, their characterization must be one of the primary objectives of the test. During the test, the modes are measured with the flight-type trunnions and latches in place and the response amplitudes are adjusted such that the loads are as representative as possible of the actual flight conditions.

The final TAM model is modifed in such a fashion that it represents an equivalent linearized model for the turnnion/latch assemblies in high amplitude. It is postulated that equivalent linearized loads model will provide a conservative loads prediction. All of the important modes producing significant loads to the payload system were measured. This provided a data base for updating the finite-element model for the final loads verification.

Acknowledgment

This research was carried out by the Jet Propulsion Laboratory, California Institute of Technology, under Contract NAS7-918. This task was monitored by Dr. James D. McAleese, Dynamics Section, NASA Lewis Research Center.

References

[1]Chen, J.C., "Analytical Model Accuracy Requirements for Structural Dynamic Systems," *Journal of Spacecraft and Rockets,* Vol. 21, July-Aug. 1984, pp. 366-373.

[2]Chen, J.C. and Wada, B.K., "Criteria for Analysis-Test Correlation of Structural Dynamic Systems," *Journal of Applied Mechanics,* Vol. 42, No. 2, June 1975, pp. 471-477.

[3]Wada, B.K., Garba, J.A., and Chen, J.C., "Development and Correlation: Viking Orbiter Analytical Dynamic Model with Modal Test," *The Shock and Vibration Bulletin*, No. 44, Pt. 2, pp. 125-164 (published by Naval Research Laboratory, Washington, DC; also published as JPL Tech. Memo. 33-690, June 1, 1974).

[4]Wada, B.K., Garba, J.A., and Chen, J.C., "Modal Test and Analysis Correlation," *Modal Testing and Model Refinement,* AMD Vol. 59, ASME, New York, Nov. 1983, pp. 85-100.

[5]Chen, J.C. and Garba, J.A., "Structural Analysis Model Validation Using Modal Test Data," *Combined Experimental/Analytical Modeling of Dynamic Structural Systems,* AMD Vol. 67, ASME, New York, June 1985, pp. 108-138.

[6]Yang, I.M. and Hruda, R.F., "Transient Response for Space Shuttle with Trunnion Friction," *Proceedings of Shuttle Payload Dynamic Environments and Loads Prediction Workshop,* Jet Propulsion Laboratory, Pasadena, CA, Jan. 1984, pp. 573-580.

[7]Henkel, E.E., Misel, J.E., and Frederick, D.H., "A Methodology to Include Static and Kinetic Friction Effects in Space Shuttle Payload Transient Loads Analysis," *Proceedings of Shuttle Payload Dynamic Environments and Loads Prediction Workshop,* Jet Propulsion Laboratory, Pasadena, CA, Jan. 1984, pp. 581-616.

[8]Chapman, J.M., "A Friction Methodology for Space Shuttle/Payload Transient Loads Analyses," *Proceedings of Shuttle Payload Dynamic Environments and Loads Prediction Workshop,* Jet Propulsion Laboratory, Pasadena, CA, Jan. 1984, pp. 543-572.